NUMERICAL SIMULATIONS OF SHOCK-ENTROPY SPOT INTERACTIONS

M.Y. Hussaini
Program in Computational Science and Engineering
Florida State University, Tallahassee, FL 32306-4052
(904) 644-0601, myh@cse.fsu.edu

G. Erlebacher
Institute for Computer Applications in Science and Engineering
Hampton, VA 23681-0001, USA
(804) 864-6781, erlebach@icase.edu

Introduction

Our continuing objective is to understand the various turbulence enhancement mechanisms, both linear and nonlinear, present in general shock-turbulence interactions [1-2]. To understand such interactions better, it is expedient to study them in isolation. To this end, there have been some theoretical studies (see references cited in [1] and [2]) of a shock interacting with an acoustic mode, a vorticity mode, and an entropy mode. In this paper, we concentrate on the mechanisms associated with the interaction of a shock with two-dimensional and axisymmetric entropy spots with particular emphasis on nonlinear effects. A previous study based on linear theory can be found in [3].

Formulation

To simulate the interaction of a shock and an entropy spot, we solve the full compressible Euler equations with a numerical algorithm which fits the shock. We choose a frame of reference in which the mean shock is steady, and the flow is from right to left. The shock forms the right boundary of the physical domain under study (see the schematic in Figure 1), and its shape $x_s(r)$ is determined along with the solution in this domain. In axisymmetric coordinates r, θ, x, the relevant governing equations are

$$\begin{aligned} \frac{\partial \mathcal{P}}{\partial t} &= -\mathbf{u}\cdot\nabla\mathcal{P} - \gamma\nabla\cdot\mathbf{u} = R_{\mathcal{P}} \\ \frac{\partial \mathbf{u}}{\partial t} &= -\mathbf{u}\cdot\nabla\mathbf{u} - T\nabla\mathcal{P} = R_{\mathbf{u}} \\ \frac{\partial s}{\partial t} &= -\mathbf{u}\cdot\nabla s \end{aligned} \tag{1}$$

where $\mathcal{P} = \log p$, p is the pressure, $\mathbf{u}$ is the velocity vector, $s = \log(p\rho^{-\gamma})$ is the entropy,

$$\nabla\cdot\mathbf{u} = \frac{\partial u_x}{\partial x} + \frac{\partial u_r}{\partial r} + \frac{u_r}{r}, \tag{2}$$

and γ is the ratio of specific heats.

These equations are supplemented by the evolution equation for the shock (see [4] for its derivation)

$$(n_x w_s)_{,t} = \frac{(F - \zeta A)(\mathbf{n} \cdot \mathbf{u}_1)_{,t} + \zeta\,(\mathbf{u} \cdot \mathbf{n}_{,t}) + (D - \zeta B)\,p_{1,t} + (E - \delta C)\,\rho_{1,t} - \mathcal{R}}{F + \zeta(1 - A)} \tag{3}$$

where A, B, C, D, E, F are functions of the upstream variables (at the shock), $\mathcal{R} = R_{\mathcal{P}} - \zeta\,\mathbf{n}_{,t} \cdot \mathbf{R}_{\mathbf{u}}$ depends on the downstream flow variables and accounts for its effect on the shock motion and $\zeta = \sqrt{\gamma/T}$, T being the downstream temperature at the shock. Note that the shock acceleration equation expressed in this form is general and can be applied to both 2-D and axisymmetric configurations.

Numerical Method

All spatial derivatives are computed using a compact 6^{th} order discretization scheme which requires the inversion of a tridiagonal matrix for each derivative evaluation [4-5]. In the presence of boundaries, the boundary point and one point removed from the boundary are computed on an explicit 8 point stencil. Time advancement is based on a low-storage, 5-stage, 4^{th} order accurate Runge-Kutta scheme. The treatment of boundary conditions at the shock, freestream and at the subsonic outflow is as follows. The Rankine-Hugoniot conditions are applied at the end of each Runge-Kutta stage to update the downstream variables at the shock. An exponentially decaying upstream temperature profile is chosen, and the freestream boundaries at the top and bottom are located 20 core radii from the center of the spot. At the left boundary (where there is subsonic outflow), a buffer domain technique described in [6] is implemented. In this approach, a finite length buffer abuts the end of the physical domain within which the convective terms in the governing equations are modified. Specifically, $\partial/\partial t$ terms are replaced by $\partial/\partial t + a(X)\partial/\partial X$, where X is the computational space coordinate. The convective velocity $a(X)$ is such that the flow is subsonic as it enters the buffer zone, and supersonic as it exits. Since the outflow is now supersonic, there is no longer any need for explicit boundary conditions. In practice, we find that the width of the buffer layer should be approximately one characteristic length. A perfectly matched layer (PML) technique developed in the context of computational electromagnetics, have been applied to the Euler equations by Hu [7]. The technique has been implemented in our algorithm and shows encouraging results [8]. In this approach, the wave reflections (in a linear problem) can be made to vanish (in theory) for all frequencies (for a given buffer width).

Results and Discussion

The spot is defined by

$$T_1'/T_1 = \epsilon\, e^{-1/2\,(x+t)^2 - 1/2\,r^2} = -\rho_1'/\rho_1, \qquad p = \text{const.}, \tag{4}$$

with a zero velocity field is an exact solution to the steady-state nonlinear Euler equations. T_1 and ρ_1 are the upstream mean temperature and density respectively. Primes denote perturbation variables. The center of the spot is at $x_0 = 1.5$, while the initial position of the shock is at $x_s = 0$. All spatial variables are normalized with respect to the spot core radius, while the non-dimensional time t^* is related to the time t via

$$t^* = -U_1 t - x_0. \tag{5}$$

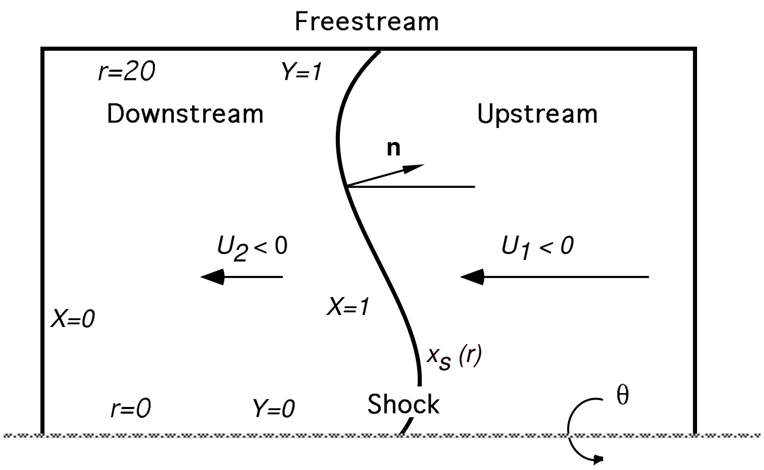

Figure 1: Axisymmetric geometry. The downstream domain is bounded by the subsonic exit $X=0$, the shock $X=1$, the symmetry axis $Y=0$ and the freestream ($Y=1$).

Therefore, the center of the spot crosses the shock at $t^*=0$, while the two edges of the spot cross the shock at $t^*=\pm 1$. The physical domain extends from the shock $x_s(r)$ to the subsonic exit located at $x=-7$. The direction parallel to the mean shock extends to $r=20$. Hereafter, we drop the $*$ from the nondimensional time t^* without causing any ambiguity.

In previous investigations [4-5], the algorithm has been extensively tested for accuracy and efficiency. In this paper, we confine ourselves to the study of enstrophy production across the shock. The enstrophy satisfies the evolution equation

$$\frac{\partial < \omega^2 >}{\partial t} = -\frac{1}{2} < \omega^2 \nabla \cdot \mathbf{u} > + < \nabla p \times \nabla \rho^{-1} \cdot \omega > - < \int_{shock} (\mathbf{u} - \mathbf{u}_s) \cdot \hat{\mathbf{n}}\, \omega^2 dl > . \quad (6)$$

Brackets denote spatial integration, $\mathbf{u}_s$ is the shock velocity, $\mathbf{u}$ is the velocity, and p and ρ are the pressure and density respectively. The vortex stretching terms are identically zero in both 2-D and axisymmetric configurations due to the absence of a spanwise and azimuthal velocity field respectively. The production of enstrophy which is directly due to the shock is given by the last term. Vorticity budgets show that this term dominates during the passage of the spot across the shock ($-2 < t < 2$). As the initial conditions are identical, the differences between 2-D and axisymmetric results are a consequence of the v/r term in the definition of the velocity divergence for axisymmetric flow. The nonlinear effects originate from two sources: the shock and the self-induced interactions. These effects are brought out in the following figures.

Figure 2 shows the time evolution of $< \omega^2 >$ at $M=2$ and $M=5$ for $\epsilon = \pm 0.25$ and 0.001 in the cases of both 2-D and axisymmetric configurations. The enstrophy is normalized by $\epsilon^2 M^2$ so that nonlinear effects are seen as departures from the $\epsilon = 0.001$ curve. For $\epsilon = -0.25$ (cold spot), there is a much stronger production of enstrophy than for $\epsilon = 0.25$ (hot spot). The reasons for this are not completely clear at present, but a heuristic argument based on the effect of the spot on the local speed of sound can be made. Inside a hot spot, the local sound speed increases by $\sqrt{1+\epsilon}$ with a corresponding decrease in the local Mach number ahead of the shock. This is consistent with the acceleration of the shock relative to the upstream spot, which is in turn consistent with a positive shock velocity near the centerline ($r = 0$). The opposite scenario occurs for the cold spot. As a result one expects that the ratio of enstrophy produced by a cold spot to that produced by a hot spot scales as

$$\frac{< \omega^2 >_{cold}}{< \omega^2 >_{hot}} \approx \frac{1 + a\epsilon}{1 - a\epsilon}. \tag{7}$$

The parameter a is a function of flow parameters such as the Mach number. It must be determined numerically, or theoretically if possible. The enhanced production of vorticity by a cold spot has been previously reported in [2]. Figure 2 also indicates that a cold 2-D spot configuration produces more enstrophy than does the axisymmetric one. This fact is not easily explained by a cursory examination of the vorticity equation. Subtle interplays between the effects of dilation and nonlinear effects on the shock motion must be responsible for this result. On the other hand the dimensionality of the spot does not seem to have an effect on the hot spot. Opposing effects must be at play to cancel the effects of the dilatational field on the vorticity production mechanism. Two-dimensional contours of vorticity along with velocity vectors are shown in Figure 3 which contrasts the effects of a low and a high Mach number shock. At $M = 5$, the deceleration of the flow as it traverses the shock is responsible for a streamwise compression of the vortex. Naturally, the sense of rotation of the vortex changes as ϵ changes sign, and the velocity vectors rotate counterclockwise for the hot spot.

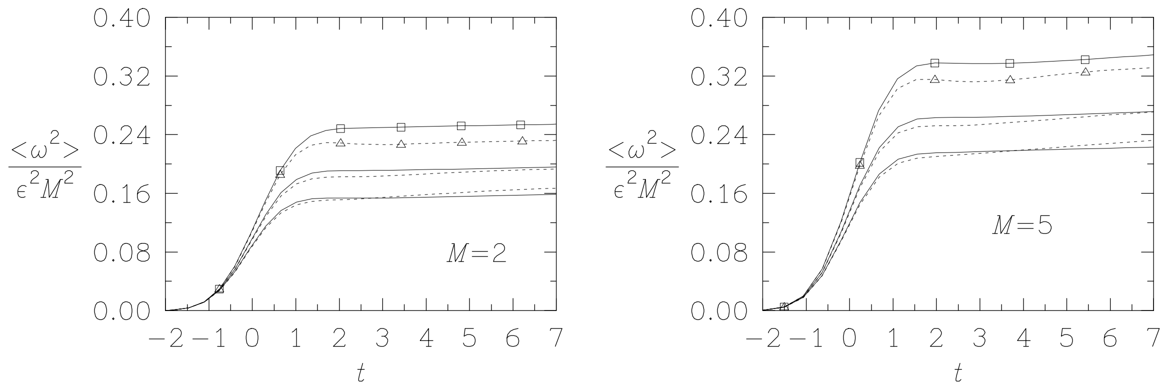

Figure 2: Time history of enstrophy at for $M = 2$ (left) and $M = 5$ (right) shock. 2D (solid), axisymmetric (dotted), 2-D cold spot (squares), axisymmetric hot spot (triangles), middle two curves are linear results ($\epsilon = 0.001$).

Additional physical insight into the differences between axisymmetric and 2-D configurations may be gained from Figure 4 which shows the time variation of the shock velocity on the centerline at $M = 2$ and $M = 5$. The particular effects of axisymmetry only become evident once the shock velocity has passed its maximum value at $t = 0$, at which point the shock slows down with respect to the 2-D case. These effects are stronger for the cold spot, and they are consistent with the enstrophy evolution in Figure 2. Although not shown here, we have confirmed that the shock velocity scales with M to leading order in the limit $M \to \infty$ while the spot crosses the shock ($t < 2$). Nonlinear effects which deviate from

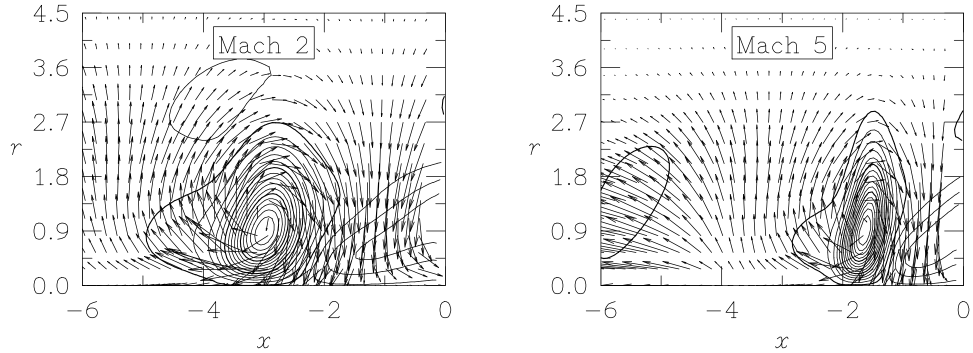

Figure 3: Azimuthal vorticity contours and velocity vector plots for a cold $M = 2$ spot (left) and a cold $M = 5$ spot (right) in a 2-D configuration. $\epsilon = -0.25$.

this high Mach number scaling are stronger for the cold axisymmetric spot. Comparisons of enstrophy at $M = 5$ and $M = 10$ indicate that the flow has reached its asymptotic scaling by $M = 5$.

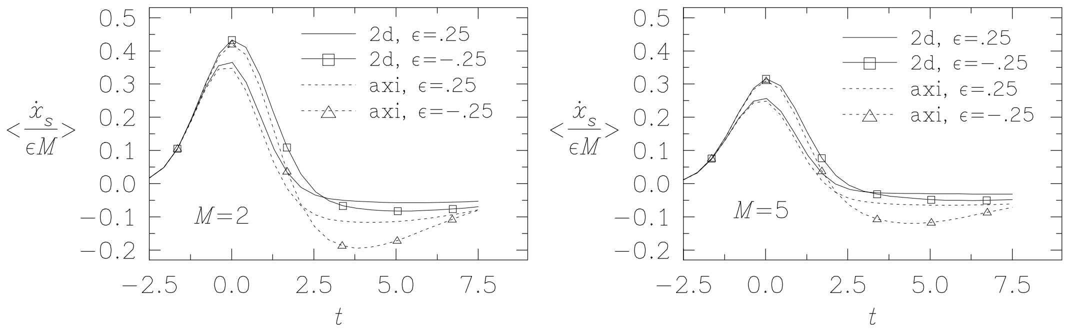

Figure 4: Time history of centerline shock velocity. $M = 2$ (left) and $M = 5$ (right) shock for 2-D flow for $\epsilon = \pm 0.25$. Cold spot curves have symbols.

The time evolution of the shock velocity profiles (in r) is shown in the two plots of Figure 5 at $t = 1$ and 4. Although at $t = 1$ the entropy spot has passed through the shock, the shock profile has not yet begun to relax to its equilibrium shape. Once the upstream disturbance has completely crossed the shock, the shock dynamics are determined by the upstream uniform flow and the information from the downstream region propagating along characteristics pointing into the shock boundary. By $t = 4$, the shock velocity profile near $r = 0$ has begun to relax to its equilibrium state $x_s(r) = 0$. Figure 6 shows the evolution of the shock position at the centerline for $M = 2$ and $M = 5$. The relaxation period appears to be shorter for the axisymmetric case compared to the 2-D one. Furthermore, the shock displacements are weaker for the stronger shocks. For a given shock Mach number, cold spots engender stronger shock displacements than the corresponding hot spots.

Conclusion

This study has revealed some effects of nonlinearity on the production of enstrophy as a shock passes across a hot or cold entropy spot. By comparing the enstrophy generation process over a range of Mach numbers it is confirmed that a cold spot interacting with a shock engenders

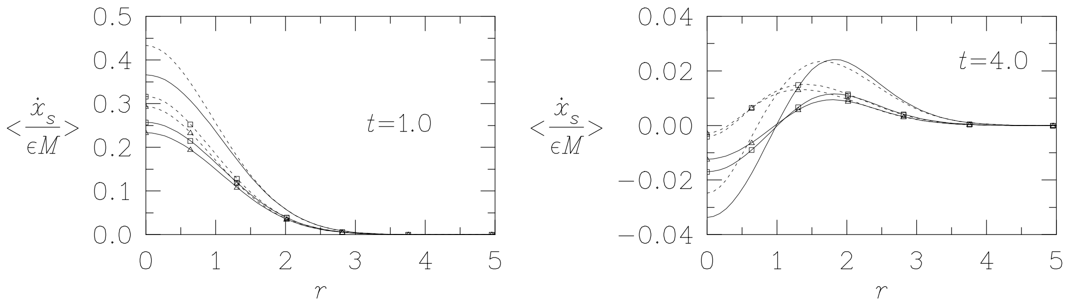

Figure 5: Shock velocity profiles at $t = 1$ (left), and $t = 4$ (right) at $M = 2, 5, 10$. $\epsilon = \pm 0.25$. Solid lines (hot spot), dotted lines (cold spot). $M = 2$ (no symbol), $M = 5$ (squares) and $M = 10$ (triangles).

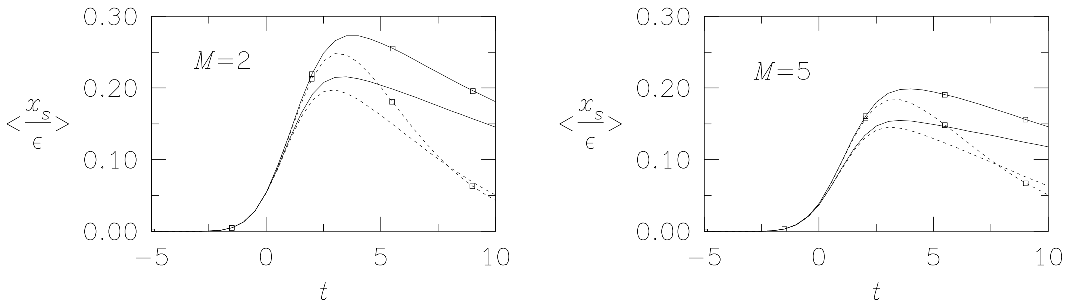

Figure 6: Time history of the shock position at the centerline at $M = 2$ (left) and $M = 5$ (right). Solid lines (2-D), dotted lines (axisymmetric). Cold spot (symbols), hot spot (no symbols).

stronger nonlinearities than a corresponding hot spot. Moreover, an axisymmetric cold spot produces less enstrophy than a corresponding 2-D one. Finally, the $\epsilon^2 M^2$ scaling of enstrophy at high spot amplitudes in the high Mach number range suggests that a theoretical study may be possible. A more detailed analysis is necessary to unravel some of the physical issues discussed here.

References

1. Hussaini, M. Y., Collier, F., and Bushnell, D.M., Turbulent Shear Layer/Shock Wave Interactions, Ed. J. Délery, Springer Verlag, (1986).
2. Zang, T. A., Hussaini, M. Y., and Bushnell, D. M., AIAA Journal **22**, No. 1, p. 13-21, (1984). See also AIAA Paper 82-0293, (1982).
3. Cuadra, E., Wyle Research Report number WR 67-17, (1968).
4. Erlebacher, G., Hussaini, M.Y., and Shu, C.-W., ICASE Report No. 96-31. Submitted to *J. Fluid Mech.*, (1996).
5. Erlebacher, G., Hussaini, M.Y., and Jackson, T.L., in preparation.
6. Ta'asan,S. & Nark, D. In *33rd Aerospace Sciences Meeting and Exhibit*, Reno, NV. AIAA Paper 95-0164, (1995).
7. Hu, F.Q. ICASE Report No. 95-70, (1995). Submitted to J. Compt. Physics.
8. Hayder, M., Hu F.Q., and Hussaini, M.Y., in preparation.